Peer-reviewed version available at *Appl. Sci.* **2020**, *10*, 3971; doi:10.3390/app10113971

Zinc Doped Halloysite Cooperating with Polylactic Acid for Bone Regeneration

Yangyang Luo[1], Ahmed Humayun[1], David K. Mills*[1, 2]

[1] *Center for Biomedical Engineering and Rehabilitation Science, Louisiana Tech University, Ruston, LA, 71272 USA*

[2] *School of Biological Sciences, Louisiana Tech University, Ruston, LA, 71272 USA*

*Corresponding author: David K. Mills, Ph.D., Center for Biomedical Engineering and Rehabilitation Sciences, and School of Biological Sciences, Louisiana Tech University, Carson Taylor Hall, Room 128
E-mail: dkmills@latech.edu; Phone (318) 257-2640; Fax (318) 257-4574

Abstract

Three-dimensional (3D) printing techniques have received considerable focus in the area of bone engineering due to its precise control in the fabrication of complex structures with customizable shapes, internal and external architectures, mechanical strength, and bioactivity. In this study, we design a new composition biomaterial consisting of polylactic acid (PLA), and halloysite nanotubes (HNTs) loaded with zinc nanoparticles (PLA+H+Zn). The hydrophobic surface of the 3D printed scaffold was coated with two layers of fetal bovine serum (FBS) on the sides and one layer of NaOH in the middle. Additionally, a layer of gentamicin was coated on the outermost layer against bacterial infection. Scaffolds were cultured in standard cell culture medium without the addition of osteogenic medium. This surface modification strategy improved material hydrophilicity and enhanced cell adhesion. Pre-osteoblasts cultured on these scaffolds differentiated into osteoblasts and proceeded to produce a type I collagen matrix and subsequent calcium deposition. 3D printed scaffolds formed from this composition possessed high mechanical strength and showed an osteoinductive potential. Furthermore, the external coating of antibiotics not only preserved the previous osteogenic properties of the 3D scaffold but also significantly reduced bacterial growth. Our surface modification model enabled the fabrication of a material surface that was hydrophilic and antibacterial, simultaneously, with an osteogenic property. The designed PLA+H+Zn may be a viable candidate for the fabrication of customized bone implants.

Keywords: Bone; 3D Printing; halloysite; PLA Surface Functionalization

1. Introduction

According to the reports of the National Ambulatory Medical Care Survey and American Academy of Orthopedic Surgeons, about 6.8 million patients ask for medical therapy due do orthopedic problems every year, and more than two million bone grafting procedures are performed annually.[1] Autografts are considered the gold standard for bone repair because of their excellent properties in osteoconduction, osteoinduction, and osteogenesis;[2] however, the concerns of limited supply, the required surgery at the site where the bone was harvested, and the risks of accompanied hematoma, infection, and additional pain from donor site afflict patients.[3] Allografts are another source for orthopedic implants, and nearly one-third of all bone grafts used in North America are allografts.[4] However, allografts are osteoconductive but with reduced osteoinductivity, which increases the risk of nonunion in fracture repair, and there is a risk of infection.[5,6] Also, the supply of allografts is limited by the long pretreatment process. Every year there remains a long list of patients waiting for receiving a bone allograft. A new method for fabricating a bone graft with proper mechanical properties, osteoconductivity, and inductivity could enhance osteogenesis is urgently needed.

Bone is a porous tissue with numerous interconnected pores that permit cell migration and proliferation, as well as vascularization;[7] therefore, an osteogenic scaffold should mimic bone morphology, structure, and function in order to ensure its integration with the native tissue. Bone implants can be produced through a variety of methods: salt leaching[8], chemical/gas foaming9, freeze-drying,[17] and sintering.[10] However, pore size, pore distribution, porosity, and pore interconnectivity cannot be precisely controlled with these approaches.[11] Three-dimensional (3D) printing technology has received considerable attention for tissue regeneration due to its superiority in the fabrication of complicated structures with tailored shapes, internal and external architecture, pre-designed microstructure, mechanical strength, and bioactivity, which can effectively mimic native tissues. With the use of osteogenic biomaterials and computer-aided design, 3D printing technology can generate a customized structure with desired features that can improve bone integration and the restoration of tissue function.[7]

Peer-reviewed version available at *Appl. Sci.* **2020**, *10*, 3971; doi:10.3390/app10113971

Hybrid materials with tunable properties have been explored in 3D printing [12–14]. Polylactic acid (PLA) is a popular material used for 3D printing medical devices. It is a thermoplastic polymer that is derived from fermented corn starch, cassava starch, or sugarcane [15]. It is an eco-friendly bioplastic as it is entirely biodegradable and consists of renewable raw materials. This material exhibits high tensile strength, low elongation, and high modulus, which enables it to be a suitable candidate for load-bearing applications, such as orthopedic fixation and sutures [15].

In this study, PLA was used to fabricate porous scaffolds through 3D printing. According to previous reports, large pore size and high porosity are key factors in producing an osteogenic response. [16–18] Therefore, we designed the scaffold with an average pore size of 600 μm and 60% porosity. PLA is a versatile, biodegradable, and FDA approved biomaterial [15], but its surface is hydrophobic and, therefore significantly reduces cell adhesion. Accordingly, surface modification to enhance its cell supportive material properties can be achieved through the addition of micro- and nanoparticles[12], fibers,[14] or fabrication of nanocomposites[13]. Halloysite is an aluminosilicate clay material $Al_2O_3 \bullet 2SiO_2 \bullet nH_2O$; it forms nanoscale tubes during the formation process. Those nanotubes are in the length of 0.5-2 μm, and with a hollow lumen that is 10-15nm in diameter, the outer diameter range between 50-80nm [19]. Halloysite nanotubes (HNTs) are cyto- and biocompatible[20]. They have attracted increasing attention in biomedical research due to its physicochemical stability, the potential for chemically modification, and ease of doping substances within its lumen, including therapeutic agents[21–24], enzymes[25], nucleic acid[26], and metal nanoparticles[27]. In addition, HNTs have been proven to enhance mechanical properties for numerous materials, such as alginate[25], chitosan[28,29], epoxy[30], nylon[24], rubber[31], and calcium phosphate[32]. Furthermore, HNTs have also been reported to chemotactically attract pre-osteoblasts[33] and enhance osteogenic differentiation[34,35].

Here, we used halloysite due to its known ability to improve polymer material properties and release bioactive agents in a sustained manner. HNTs were loaded with zinc nanoparticles. Zinc is one of the essential minerals that play an essential role in bone health. It affects multiple enzyme activities, collagen synthesis[36], and DNA synthesis[37], and it has been demonstrated to stimulate bone metabolism[38]. Then, the zinc-loaded HNTs mixed with PLA for 3D printing. Fetal

Bovine Serum (FBS) and NaOH were used to improve the surface hydrophilicity of a3D printed scaffold. Scaffold mechanical properties and cell-material interactions were studied. We also coated the 3D printed scaffold with antibody, gentamicin, to prevent contamination and assessed the drug efficiency after three weeks. This study aims to generate a 3D printed scaffold to support bone regeneration and prevent bacterial contamination, which may be potentially used for bone defect therapy in the clinic.

2. Materials and Methods

2.1 Zinc Loaded into HNTs

Zinc nanoparticles (NPs) were deposited on the HNT surface by thermal decomposition of the metal acetate, as depicted in Figure 1. Zinc oxide (ZnO) reacted with acetic acid at 50°C with continuous stirring, then the mixture was heated to a boil, and the reaction continued for 12 hours, with additional acetic acid added during this time period. The resulting zinc acetate ($Zn(OAc)_2$) was filtered using Whatman #1 filter paper[39]. Then, 20g of $Zn(OAc)_2$ mixed with 10g of HNTs in 50 ml DI water and stirred for 12 hours. After centrifugation, the pellet was collected and heated at 350°C for 2 hours, which led to thermal decomposition of the metal acetate on HNTs surface (ZnO-HNTs) [40].

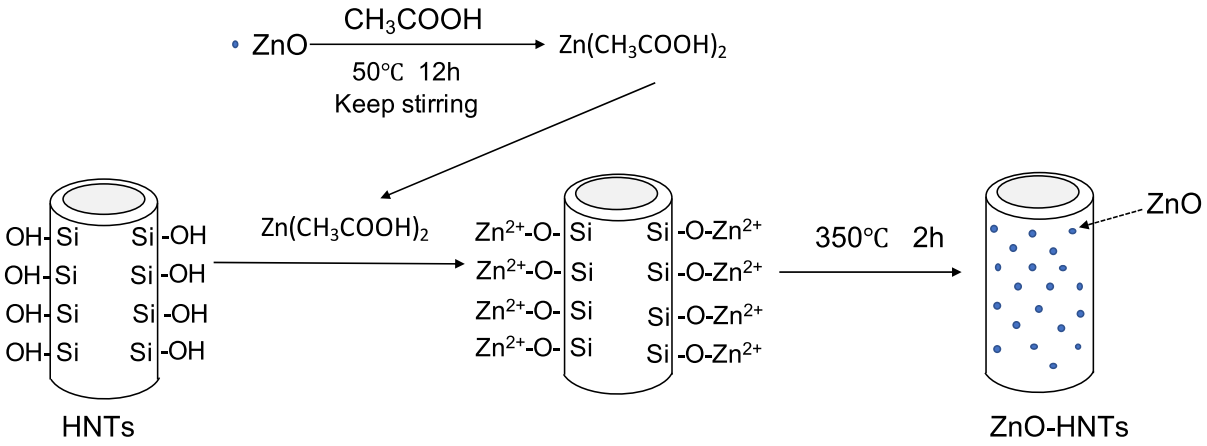

Figure 1. Facile synthesis and characterization of ZnO nanoparticles grown on halloysite nanotubes for enhanced photocatalytic properties.

2.2 Material Preparation

Four composition were tested in this study: PLA, PLA+HNTs, PLA+HNTs/Zn, and PLA+HNTs/Zn+gentamicin. These groups were printed using an ENDER 3 printer with similar

setting; however, different filament compositions were used. Filaments were extruded using a Noztek Pro Extruder (West Sussex, England) with a uniform diameter 1.75±0.05mm, but there was slightly different in filaments preparation for each group. For PLA group, PLA filaments were extruded at 175°C. For PLA+HNTs group, in order to archive a uniform distribution of HNTs in PLA, 10 µl of silicon oil was added into 20g PLA and vortexed for 10 minutes, then 1.2g of HNTs were added and continually vortexed for another 10 minutes. Then mixture of PLA+HNTs were extruded at 170°C. Filaments of PLA+HNTs/Zn prepared similarly as PLA+HNTs; the only difference is HNTs were loaded with Zn (30% w/w) and extruded at 165 °C. PLA+HNTs/Zn+gentamicin scaffolds were printed with PLA+HNTs/Zn filaments, and then they dipped into a 100mg/ml gentamicin solution for 24 hours.

2.3 3D Printing

All filaments types were 3D printed into a pre-designed structure (squares) using an ENDER 3 printer at 225°C. The squares were designed to be 6×6×2 mm with a pore size of 0.6mm (Figure 2). The diameter of inside lattice supports was 0.6mm.

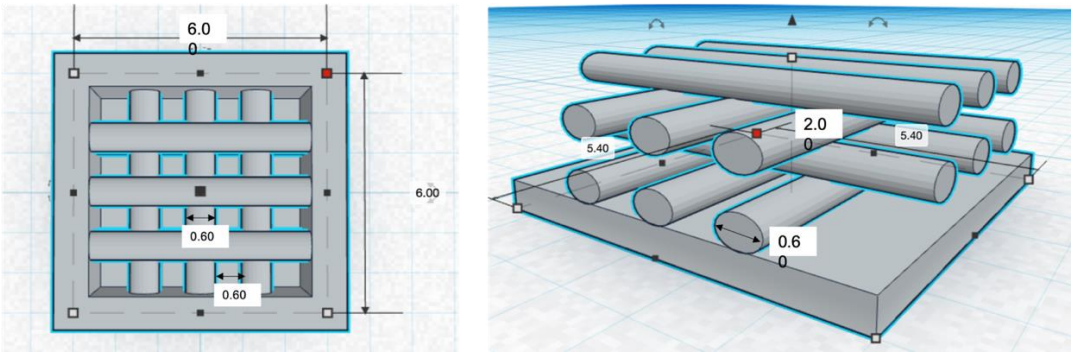

Figure 2. CAD drawing of the 3D printing square and design specifications.

2.4 Porosity

The porosity of the 3D printed disks was calculated through liquid displacement. One 3D square was immersed into 1.0 ml (V1) of DI water, then a series of vortexing and sonication was applied to force the liquid into the pores. The total volume of square and DI water was

Peer-reviewed version available at Appl. Sci. 2020, 10, 3971; doi:10.3390/app10113971

measured (V2), after the water was removed, the square and the remaining volume of DI water was measured (V3). The final porosity of the square was calculated as below:

$$\text{porosity} = \frac{V1 - V3}{V2 - V3}$$

2.5 Compression Testing

A Univert CellScale Testing device (Waterloo, Ontario, Canada) was used for compression test of the printed squares. 3D printed squares were compressed at a speed of 10 mm/min with a 200 N load cell. The strain and stress profiles were recorded. A minimum of 3 tests were performed for each composition.

2.6 Surface Treatment of 3D Printed Square

According to the pilot study (Supplementary information), a sandwich coating (Figure 3) on the 3D printed squares was shown to significantly improve the surface hydrophilicity and facilitate cell adhesion. Therefore, we coated the 3D printed disk for three layers. For the first layer, each square was immerged in fetal bovine serum (FBS) for 24 hours; then each square was immerged into 10 N NaOH for 30 minutes and washed three times with sterilized DI water; for the last layer, squares were incubated in FBS again for 24 hours. Squares with a three-layer sandwich-like coating were labeled as FBS+NaOH+FBS.

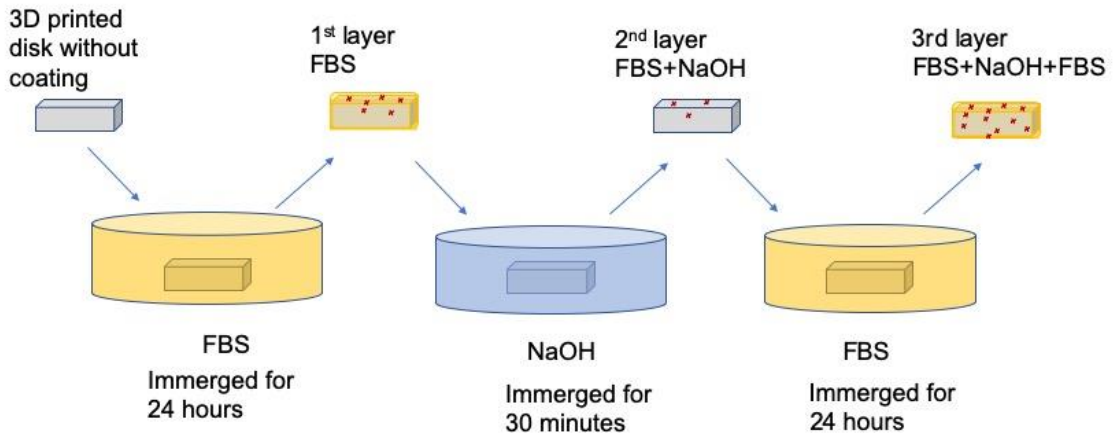

Figure 3. The process of applying the three-layered coating onto 3D printed squares.

2.7 Morphology and Surface Characterization

The morphology of 3D printed disks was observed using a scanning electron microscope (SEM) and laser confocal microscope. The distribution of HNTs and HNTs/Zn in the PLA filament

was observed by Energy Dispersive Spectrometer (EDS) using a PLA filament in cross-section. The presence and nature of the surface coating was also determined by EDS.

2.8 Cell Proliferation

Surface modified squares were put into 48 wells plate, each well had one square and seeded with pre-osteoblast (MC3T3-E1, ATCC, Manassas, VA) at a cell density of 1×10^5/well. Then, the cells were cultured in alpha modification of Eagle's medium (α-MEM, Hyclone, GE Life Sciences) with 10% fetal bovine serum (FBS) and 1% Pen/Strep antibiotic (Life Technologies Corporation) in a humidified incubator at 37 °C and 5% CO_2. An MTS (BioVision, USA) was used to assess cell proliferation. A stock solution (40 ul) were added to each well and incubated at 37°C in darkness for 2 hours. After then, 200ul of supernatant was taken to measure absorbance value at wavelength of 490 nm.

2.9 Mineralization-Alizarin Red Staining

Matrix mineralization was assessed through Alizarin Red S (ARS) staining. Cells culture on the 3D printed squares were fixed with 4% paraformaldehyde for 15 minutes at room temperature, then stained with 2% ARS for 30 minutes. Then, all squares were washed by DI water 4 times and observed under an Olympus BX41 light microscope. Cells cultured in monolayer were used as control.

2.10 Picrosirius Red Staining

Picrosirius Red is a specific collagen fiber stain that is capable of detecting thin collagenous fibers. The media was aspirated from the cell culture plates, and each culture well was washed with DPBS before being fixed in 4% paraformaldehyde. Fixed cells were stained with Picrosirius Red to quantify the amount of collagen secreted. Picrosirius stain was added to each well and removed after an hour incubation at room temperature. The cells were rinsed with 0.5% acetic acid solution twice and absolute alcohol twice. Digital images of stained squares were acquired using a brightfield microscope. Cells cultured in monolayer were used as control.

2.11 Antibacterial Efficiency

The antibacterial ability of PLA+HNTs/Zn+gentamicin squares against *Staphylococcus aureus* (*S.aureus*) was assessed. 3D printed squares were placed in 24-well cell culture plate and each well was inoculated with 1ml *S.aureus* (0.3×10^7 CFU/ml). The *S.aureus* was sub-cultured from a

single colony and maintained in Muller Hinton broth. The plate was incubated in horizontal orbital microplate shaker at 37°C for 12 hours. The absorbance of the incubation solution at 630nm was measured. Muller Hinton broth without PLA+HNTs/Zn+gentamicin squares and *S.aureus* set as negative and positive control, respectively.

2.12 Statistical Analysis

A one-way ANOVA or Student T-test was used for statistical analysis. Data were expressed as mean ± standard error. A p-value less than 0.05 was considered statistically significant.

3. Results and Discussion

3.1 Distribution of HNTs and Zinc Nanoparticles in the PLA Filament

Filaments used to print PLA+HNTs, and PLA+HNTs/Zn squares were prepared by mixing PLA with HNTs or zinc-coated HNTs (HNTs/Zn). In order to determine whether the HNTs or HNTs/Zn were distributed throughout the PLA, filament cross-sections were analyzed with EDS. In Figure 4, all pictures represent the same visual field but present different elements. The primary element of PLA is carbon (C), which is exhibited all over the screen. Silicon (Si) and aluminum (Al) are the two major elements of HNTs, according to the graph, they were well distributed in the PLA filament. Zinc nanoparticles were coated into HNTs with 30% w/w, its distribution was detected by EDS as well. According to the EDS analysis, HNTs and HNTs/Zn were well distributed throughout the PLA filament.

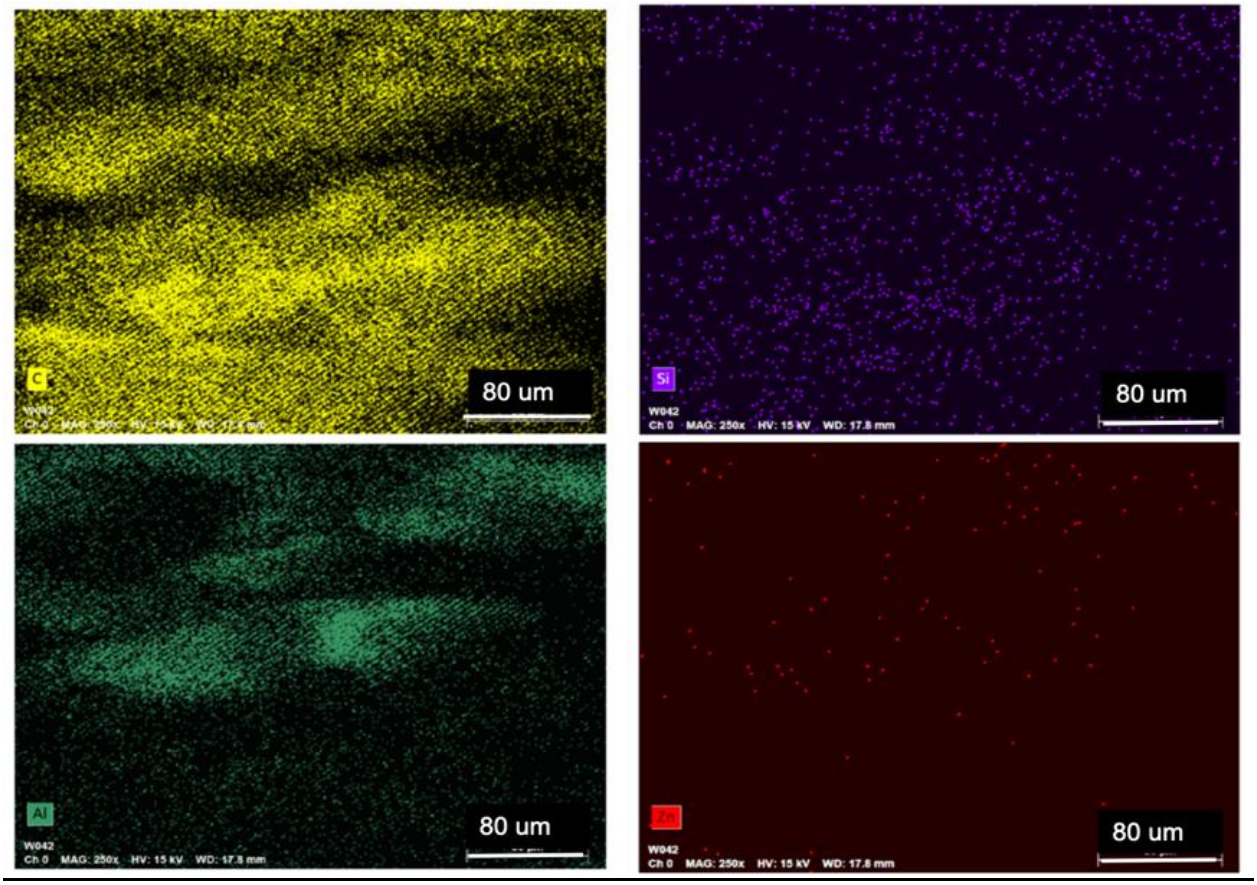

Figure 4. EDS analysis of PLA+HNTs/Zn filament cross-section. All four pictures were focused on the same area, and each picture exhibits one element. Four elements were present. They are carbon (C), silicon (Si), aluminum (Al), and zinc (Zn).

3.2 Morphology of 3D printed Squares and their Surface Characteristics

All filaments were printed into a pre-designed square with a pore size of 600 μm x 600 μm and a layer height of 600 μm (Figure 2). Due to the limitations of the 3D printer used, the resolution changed slightly during printing. The exact pore size was determined using a laser confocal microscope (Figure 5). Based on the measurement of 60 pores from 20 different scaffolds, the average pore size of printed scaffolds is 584.16±95.28 μm x 620.39±93.03 μm and with a porosity of 60.22±9.5%.

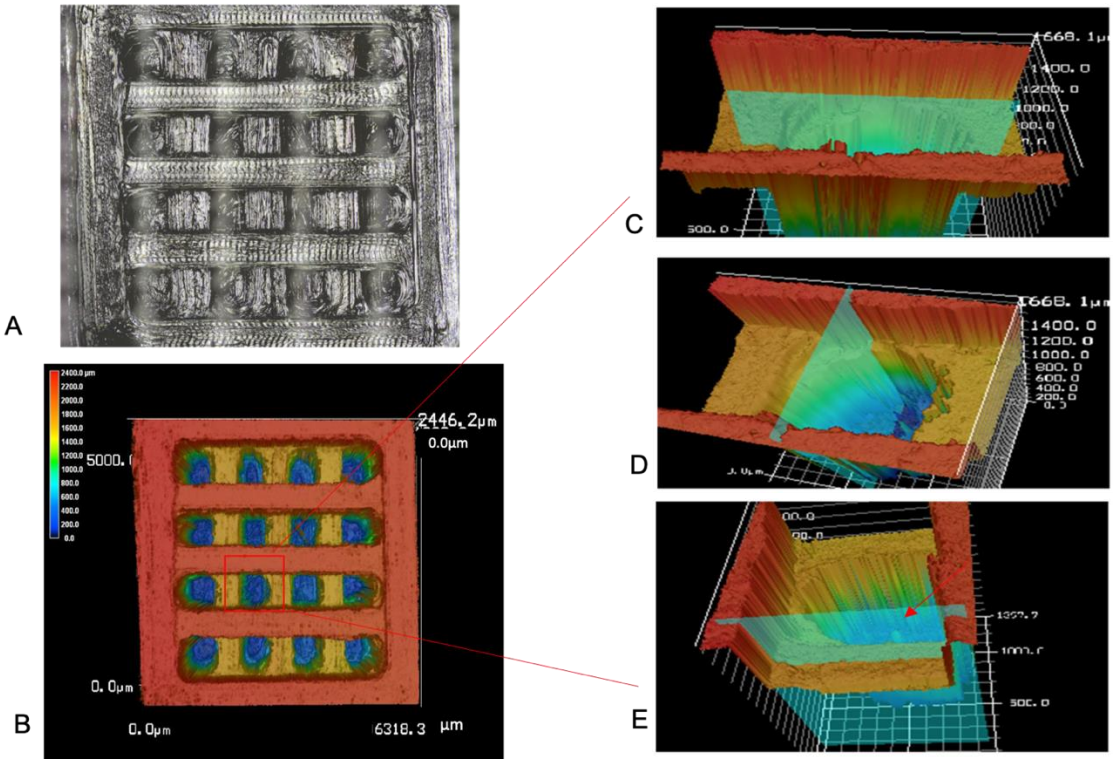

Figure 5. A. Optical and laser combined picture of 3D printed square. B. Laser confocal image of 3D printed square. C. Horizontal section of selected pore, the horizontal distance was measured (584.16±95.28 μm, n=60). D. Vertical section of selected pore, the vertical distance was measured (620.39±93.03μm, n=60). E. Vertical section of selected pore, the layer thickness was measured (423.15±82.7μm, n=60).

3.3 Compressive Strength

In order to evaluate the contribution of HNTs towards the enhancement of PLA's mechanical properties in the printed squares, the compressive strength of 3D printed scaffolds was analyzed, with and without HNTs addition. However, due to the limitation of the testing instrument, no scaffolds broke after the application of the maximum force (200N). Scaffolds with HNTs (PLA+H and PLA+H+Zn) did have a higher strain percentage and higher average compressive modulus as compared to the squares without HNTs (PLA only), indicating that the addition of HNTs only contributed a slight enhancement to the elasticity and compressive strength of PLA (Figure 6).

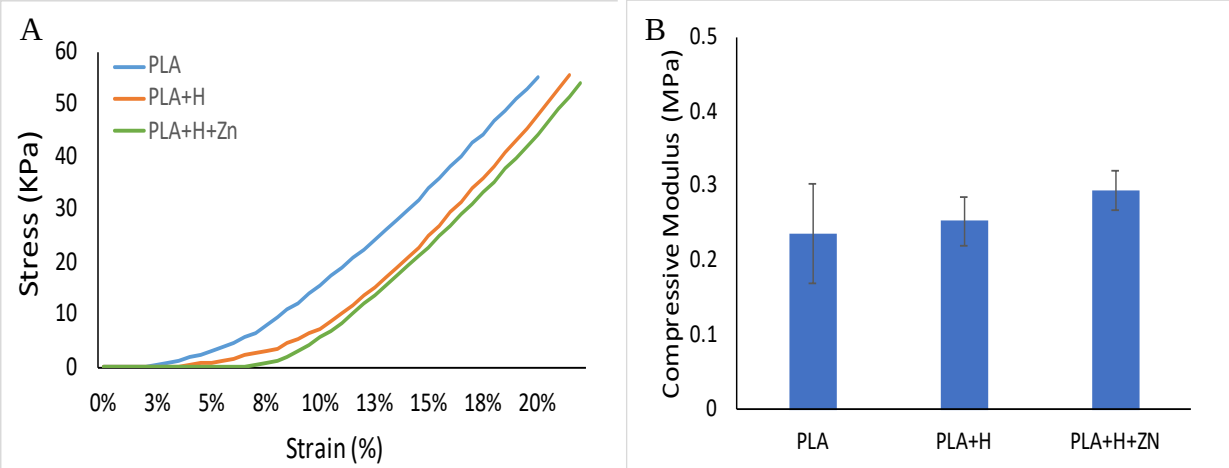

Figure 6. (A) Stress vs. Strain profile and the compressive modulus of PLA, PLA+H, and PLA+H+Zn. (B) The compressive modulus: PLA=0.24±0.07 MPa, PLA+H=0.25±0.03 MPa, PLA+H+Zn=0.29±0.03 MPa. (error bar with standard deviation, n=5).

3.4 Chemical Deposition

After processing the sandwich-like layered surface modification, the hydrophilicity of the printed squares was significantly improved (Supplementary Figure 1). In our hypothesis, surface hydrophilicity would keep increasing with each layer modification. However, the hydrophilicity decreased after the second layer modification was treated with NaOH, and then the hydrophilicity significantly increased after the third layer was added (Supplementary data, Figure 1). This phenomenon may have occurred because the NaOH eroded the chemicals that were deposited in the first layer modified with FBS. However, simultaneously, this erosion produced more links for chemical deposition, which lead to increased chemical deposition after the addition of the third layer (supplementary Figure 2, 3, and Figure 7).

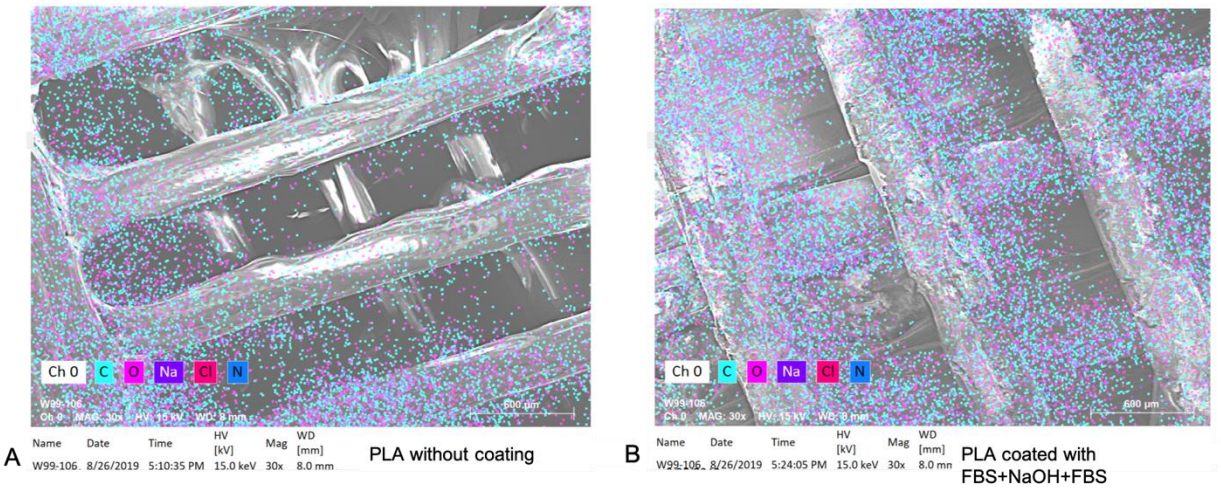

Figure 7. The EDS elemental analysis for PLA square with a naked surface (A) and a sandwich-like coating (B).

3.5 Antibacterial Studies

FBS contains many substances which may lead to the growth of undesired microorganism; therefore, we coated the PLA+H+Zn with gentamicin (PLA+H+Zn+G). Gentamicin is an efficient antibiotic against gram-positive and negative bacteria41. Even though they were stored at 37°C for three weeks, they still efficiently inhibited bacterial growth (Figure 8). As expected, printed squares without gentamicin showed no bacterial growth inhibition.

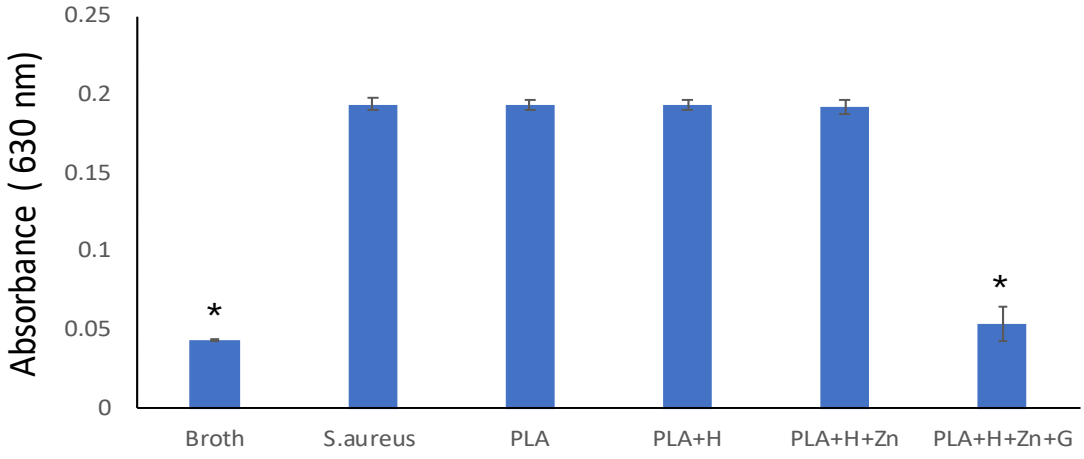

Figure 8. Bacterial growth inhibition. Broth without any samples or bacterial were set as the negative control (Broth). *S.aureus* culture in broth was set as the positive control (*S.aureus*). The same amount of *S.aureus* suspension was co-cultured with a scaffold composed by PLA, PLA added with HNTs (PLA+H), PLA added with zinc-loaded HNTs (PLA+H+Zn), and PLA added with zinc-loaded HNTs and coated with gentamicin (PLA+H+Zn+G). (error bar with standard deviation, n=3, $p<0.05$).

Peer-reviewed version available at Appl. Sci. 2020, 10, 3971; doi:10.3390/app10113971

3.6 Response of Pre-Osteoblast to 3D Printed Squares

Cell Proliferation

Many studies have shown that surface features, such as charge[42,43], roughness[44], adsorbed proteins, and hydrophilicity/hydrophobicity[45], greatly influenced cell attachment and subsequent cell behaviors. Our results consist with previous studies, cell adhesion was improved with hydrophilicity and increased protein attachment (supplementary data, Figure 4). In addition, cells preferred to proliferate on 3D squares as compared to than monolayer cultures (Figure 9).

The influence of gentamicin on cell proliferation was also assessed. Consistent with the study of Philip et.al[46], the presence of gentamicin did induce a small but transient effect on cell proliferation (Figure 9). However, the presence of gentamicin did not have a negative effect on mineralization (Figure 10).

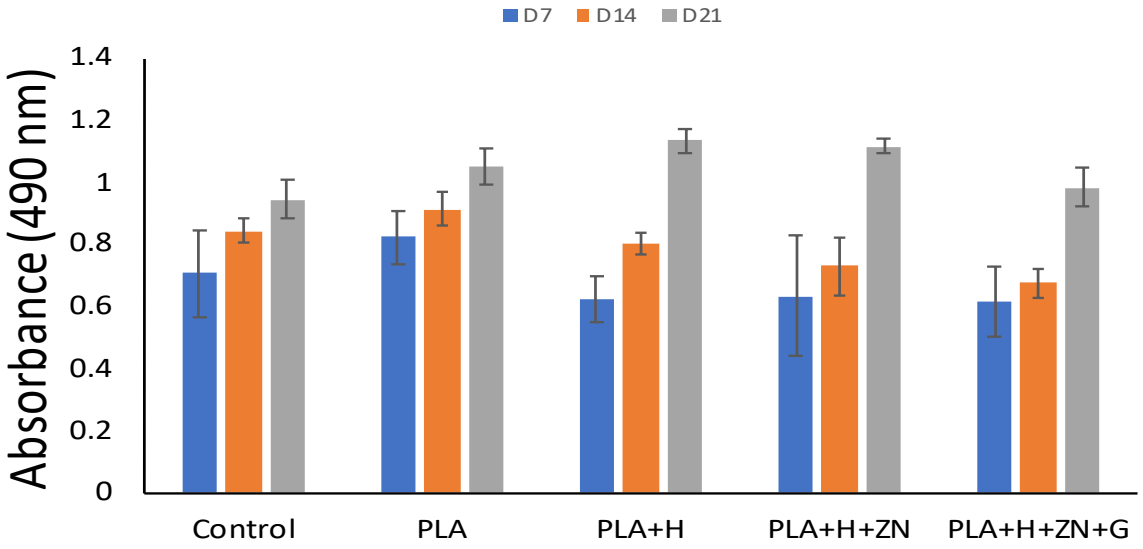

Figure 9. Cell proliferation in 21 days incubation. Cell cultured in monolayer culturing set as control. Then cells cultured with 3D squares consisted of 4 compositions: PLA, PLA added with HNTs (PLA+H), PLA added with zinc-loaded HNTs (PLA+H+Zn), and PLA added with zinc-loaded HNTs and coated with gentamicin (PLA+H+Zn+G). (error bar with standard deviation, n=5, $p<0.05$).

Bone formation

Bone consists of bone cells and a mineralized collagenous matrix [47,48]. The main constituents of the bone matrix are hydroxyapatite [$Ca_{10}(PO_4)6(OH)2$] (50-70%) and an organic matrix (20-40%).[49] Type I collagen is the major component of bone tissue extracellular matrix (ECM), which

Preprints (www.preprints.org) | NOT PEER-REVIEWED | Posted: 9 May 2020 doi:10.20944/preprints202005.0165.v1

Peer-reviewed version available at Appl. Sci. 2020, 10, 3971; doi:10.3390/app10113971

is mainly synthesized by osteoblasts. The synthesis of type I collagen is one of the markers of osteogenic differentiation[50]. Processed with Picrosirius Red staining, type III collagen stained red, and type I collagen stained yellow. In the first 7 days incubation, collagen secretion by cells in monolayer culture was negligible. In contrast, type III collagen synthesized by cells cultured on different 3D square compositions was very apparent (Supplementary information Figure 5).

Furthermore, compared to the inner space, more type III collagen was synthesized on the bottom surface of the square, and the transformation from type III collagen to type I collagen happened earlier on the bottom surface of the well (Supplementary data Figure 5 vs. Figure 6). Osteoblast differentiation in 3D scaffolds usually spreads from the scaffold periphery and gradually proceeds into the inner scaffold space[51]. Similar to the results seen with collagen synthesis, after 21 days of incubation, there was increased calcium deposition in the 3D scaffolds as compared to cells in monolayer culture (Figure 10). Calcium deposition indicates mineralization of the bone matrix, which is another marker for bone tissue formation. Alizarin Red S stained the calcium deposited in the collagenous matrix (red), which was rarely found in monolayer culture after 7 days of incubation (Supplementary data Figure 7).

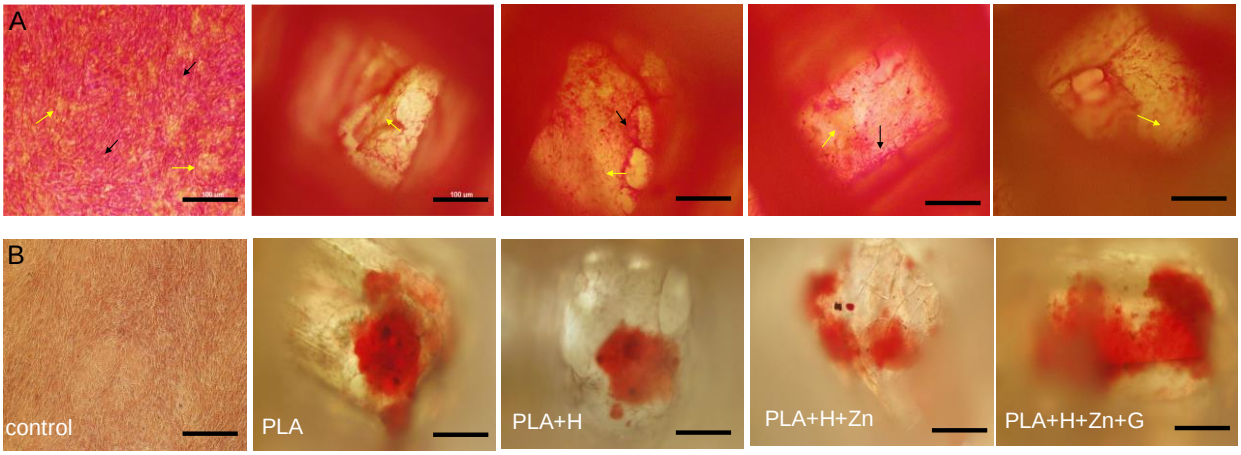

Figure 10. **(**A). Picrosirius Red Stain for bottom layer of 3D squares after 21 days incubation. The red color represents type III collagen (black arrows) and yellow color represents type I collagen (yellow arrows). Cells incubated in monolayer set as control (fare left figures). (B). Alizarin Red stain for calcium deposition after 21 days incubation. (scale bar is 100 µm)

4. Conclusion

In this study, we 3D printed squares composed of PLA and zinc doped HNTs for use as a potential bone implant. The material's porosity mimicked that of human bone tissue. When a

unique sandwich coating of FBS+NaOH+FBS was applied to the printed squares, hydrophilicity was enhanced that facilitated cell adhesion and proliferation. Sandwich-coated PLA squares were also osteoinductive as seeded pre-osteoblasts differentiated into osteoblasts without the addition of exogenous osteogenesis agents. Also, an external coating of gentamicin reduced the risk of infection without negatively influencing osteogenesis. The newly designed hybrid material, PLA+H+Zn, also possessed good mechanical strength and osteoinductivity and may serve as a candidate for 3D printing of bone implants. Furthermore, the surface modification strategy used in this study may also be used for other 3D printing applications.

Acknowledgments: Funding for this study was provided by a grant (to DKM) from the Louisiana Biomedical Research Network (through an Institutional Development Award (IDeA) from the National Institute of General Medical Sciences of the National Institutes of Health under grant number P20 GM103424-17. The authors also wish to acknowledge the support of the College of Applied and Natural Sciences (Louisiana Tech University) Matching Grant Program.

Author Contributions: The authors all contributed to the writing of the manuscript. A.H. conducted the experiments under the direction of D.K.M. Both authors reviewed and analyzed the data.

Declaration of Interest: DKM has received a patent on an electrolytic method for metalizing halloysite nanotubes (U.S. Patent No. 9,981,074).

References:

1. Campana V, Milano G, Pagano E, et al. Bone substitutes in orthopaedic surgery: from basic science to clinical practice. *J Mater Sci Mater Med*. 2014;25:2445-2461. doi:10.1007/s10856-014-5240-2
2. Bauer TW, Muschler GF. Bone graft materials. An overview of the basic science. *Clin Orthop Relat Res*. 2000;371:10-27.
3. Sanchez CJ, Ward CL, Romano DR, et al. Staphylococcus aureus biofilms decrease osteoblast viability, inhibits osteogenic differentiation, and increases bone resorption in vitro. *BMC Musculoskelet Disord*. 2013;14:187. doi:10.1186/1471-2474-14-187
4. De Long WG, Einhorn TA, Koval K, et al. Bone grafts and bone graft substitutes in orthopaedic trauma surgery: A critical analysis. *J Bone Jt Surg - Ser A*. 2007:649-658. doi:10.2106/00004623-200703000-00026
5. Hatzenbuehler J, Pulling TJ. Diagnosis and Management of Osteomyelitis - American Family Physician. *Am Fam Physician*. 2011;84(9):1027-1033. doi:10.2165/00019053-199916060-00003
6. Burge R, Dawson-Hughes B, Solomon DH, Wong JB, King A, Tosteson A. Incidence and economic burden of osteoporosis-related fractures in the United States, 2005-2025. *J Bone Miner Res*. 2007;22:465-475. doi:10.1359/jbmr.061113
7. Karageorgiou V, Kaplan D. Porosity of 3D biomaterial scaffolds and osteogenesis. *Biomaterials*. 2005;26(27):5474-5491. doi:10.1016/j.biomaterials.2005.02.002
8. Cao H, Kuboyama N. A biodegradable porous composite scaffold of PGA/β-TCP for bone tissue engineering. *Bone*. 2010;46(2):386-395. doi:10.1016/j.bone.2009.09.031
9. Kucharska M, Butruk B, Walenko K, Brynk T, Ciach T. Fabrication of in-situ foamed chitosan/β-TCP scaffolds for bone tissue engineering application. *Mater Lett*. 2012;85:124-127. doi:10.1016/j.matlet.2012.07.002
10. Sultana N, Wang M. Fabrication of HA/PHBV composite scaffolds through the emulsion freezing/freeze-drying process and characterisation of the scaffolds. In: *Journal of Materials Science: Materials in Medicine*. ; 2008:19:2555. doi:10.1007/s10856-007-3214-3
11. Bose S, Vahabzadeh S, Bandyopadhyay A. Bone tissue engineering using 3D printing.

Mater Today. 2013:16, 12, 496-504. doi:10.1016/j.mattod.2013.11.017

12. Nikzad M, Masood SH, Sbarski I. Thermo-mechanical properties of a highly filled polymeric composites for Fused Deposition Modeling. *Mater Des*. 2011;32(6):3448-3456. doi:10.1016/j.matdes.2011.01.056
13. Gu J, Li N, Tian L, Lv Z, Zhang Q. High thermal conductivity graphite nanoplatelet/UHMWPE nanocomposites. *RSC Adv*. 2015;5(46):36334-36339. doi:10.1039/c5ra03284a
14. Zhong W, Li F, Zhang Z, Song L, Li Z. Short fiber reinforced composites for fused deposition modeling. *Mater Sci Eng A*. 2001;301(2):125-130. doi:10.1016/S0921-5093(00)01810-4
15. Middleton JC, Tipton AJ. Synthetic biodegradable polymers as orthopedic devices. *Biomaterials*. 2000;21:2335-2346. doi:10.1016/S0142-9612(00)00101-0
16. Jin QM, Takita H, Kohgo T, Atsumi K, Itoh H, Kuboki Y. Effects of geometry of hydroxyapatite as a cell substratum in BMP- induced ectopic bone formation. *J Biomed Mater Res*. 2000;51(3):491-499. doi:10.1002/1097-4636(20000905)51:3<491::AID-JBM25>3.0.CO;2-1
17. Xue W, Krishna BV, Bandyopadhyay A, Bose S. Processing and biocompatibility evaluation of laser processed porous titanium. *Acta Biomater*. 2007;3(6):1007-1018. doi:10.1016/j.actbio.2007.05.009
18. Otsuki B, Takemoto M, Fujibayashi S, Neo M, Kokubo T, Nakamura T. Pore throat size and connectivity determine bone and tissue ingrowth into porous implants: Three-dimensional micro-CT based structural analyses of porous bioactive titanium implants. *Biomaterials*. 2006;27(35):5892-5900. doi:10.1016/j.biomaterials.2006.08.013
19. Darrat Y, Naumenko E, Cavallaro G, Lazzara G, Lvov Y. Tubular nanocontainers for drug delivery. In: *Materials Nanoarchitectonics*. ; 2018:85-108.
20. Li LY, Zhou YM, Gao RY, et al. Naturally occurring nanotube with surface modification as biocompatible, target-specific nanocarrier for cancer phototherapy. *Biomaterials*. 2019;190:86-96. doi:10.1016/j.biomaterials.2018.10.046
21. Dionisi C, Hanafy N, Nobile C, et al. Halloysite clay nanotubes as carriers for curcumin: Characterization and application. *IEEE Trans Nanotechnol*. 2017;15(5):720-744.

doi:10.1109/TNANO.2016.2524072

22. Liu M, Chang Y, Yang J, et al. Functionalized halloysite nanotube by chitosan grafting for drug delivery of curcumin to achieve enhanced anticancer efficacy. *J Mater Chem B*. 2016;b4:2253-2263. doi:10.1039/c5tb02725j
23. Shin JM, Kim SH, Thambi T, et al. A hyaluronic acid-methotrexate conjugate for targeted therapy of rheumatoid arthritis. *Chem Commun*. 2014;50(57):7632-7635. doi:10.1039/c4cc02595d
24. Sun L, Boyer C, Grimes R, Mills DK. Drug Coated Clay Nanoparticles for Delivery of Chemotherapeutics. *Curr Nanosci*. 2015;12(2):207-214. doi:10.2174/1573413711666151008014051
25. Karnik S, Hines K, Mills DK. Nanoenhanced hydrogel system with sustained release capabilities. *J Biomed Mater Res - Part A*. 2015;103A:2416-2426. doi:10.1002/jbm.a.35376
26. Shi YF, Tian Z, Zhang Y, Shen HB, Jia NQ. Functionalized halloysite nanotube-based carrier for intracellular delivery of antisense oligonucleotides. *Nanoscale Res Lett*. 2011;6(1):608. doi:10.1186/1556-276X-6-608
27. Nicholson JC, Weisman JA, Boyer CJ, Wilson CG, Mills DK. Dry sintered metal coating of halloysite nanotubes. *Appl Sci*. 2016;6(9):265. doi:10.3390/app6090265
28. Luo, Mills. The Effect of Halloysite Addition on the Material Properties of Chitosan–Halloysite Hydrogel Composites. *Gels*. 2019;5(3):40. doi:10.3390/gels5030040
29. Liu M, Wu C, Jiao Y, Xiong S, Zhou C. Chitosan-halloysite nanotubes nanocomposite scaffolds for tissue engineering. *J Mater Chem B*. 2013;1(15):2078-2089. doi:10.1039/c3tb20084a
30. Liu M, Guo B, Du M, Cai X, Jia D. Properties of halloysite nanotube-epoxy resin hybrids and the interfacial reactions in the systems. *Nanotechnology*. 2007;18(45):455703. doi:10.1088/0957-4484/18/45/455703
31. Rooj S, Das A, Thakur V, Mahaling RN, Bhowmick AK, Heinrich G. Preparation and properties of natural nanocomposites based on natural rubber and naturally occurring halloysite nanotubes. *Mater Des*. 2010;31(4):2151-2156. doi:10.1016/j.matdes.2009.11.009

32. Tappa KK, Jammalamadaka UM, Mills DK. Design and evaluation of a nanoenhanced anti-infective calcium phosphate bone cements. In: *2014 36th Annual International Conference of the IEEE Engineering in Medicine and Biology Society, EMBC 2014*. ; 2014:3921-3924. doi:10.1109/EMBC.2014.6944481

33. Li Y, Mills DK. Halloysite nanotubes as a potential chemotactic agent for bone repair. In: *Orthopedic Research Society Meeting, Phoneix, AX*.

34. Udayabhanu J, Karthik T, Mills, David K. Calcium phosphate/clay nanotube bone cement with enhanced mechanical properties and sustained drug release. In: *In Caly Science and Engineering, Dr. Mansoor Zoveidavianpoor, Editorl*.

35. Huang K, Ou Q, Xie Y, et al. Halloysite Nanotube Based Scaffold for Enhanced Bone Regeneration. *ACS Biomater Sci Eng*. 2019;5(8):4037-4047. doi:10.1021/acsbiomaterials.9b00277

36. Tengrup I, Ahonen J, Zederfeldt B. Influence of zinc on synthesis and the accumulation of collagen in early granulation tissue. *Surg Gynecol Obstet*. 1981;152(3):323-326.

37. Yamaguchi M, Yamaguchi R. Action of zinc on bone metabolism in rats. Increases in alkaline phosphatase activity and DNA content. *Biochem Pharmacol*. 1986;35:773. doi:10.1016/0006-2952(86)90245-5

38. Yamaguchi M, Oishi H, Suketa Y. Stimulatory effect of zinc on bone formation in tissue culture. *Biochem Pharmacol*. 1987;36:4007. doi:10.1016/0006-2952(87)90471-0

39. Poshkus AC. Improved synthesis of basic zinc acetate, hexakis (. mu.-acetato)-. mu.-oxotetrazinc. *Ind Eng Chem Prod Res Dev*. 1983;22(2):380-381.

40. Peng H, Liu X, Tang W, Ma R. Facile synthesis and characterization of ZnO nanoparticles grown on halloysite nanotubes for enhanced photocatalytic properties. *Sci Rep*. 2017;7(1):2250.

41. Gonzalez LS, Spencer JP. Aminoglycosides: A practical review. *Am Fam Physician*. 1998;58(8):1811-1820.

42. Shelton RM, Rasmussen AC, Davies JE. Protein adsorption at the interface between charged polymer substrata and migrating osteoblasts. *Biomaterials*. 1988;9:24-29. doi:10.1016/0142-9612(88)90065-8

43. van Wachem PB, Hogt AH, Beugeling T, et al. Adhesion of cultured human endothelial

cells onto methacrylate polymers with varying surface wettability and charge. *Biomaterials*. 1987;8:323-328. doi:10.1016/0142-9612(87)90001-9

44. Chehroudi B, Gould TRL, Brunette DM. Titanium-coated micromachined grooves of different dimensions affect epithelial and connective-tissue cells differently in vivo. *J Biomed Mater Res*. 1990;24:1202-1219. doi:10.1002/jbm.820240906
45. Webb K, Hlady V, Tresco PA. Relative importance of surface wettability and charged functional groups on NIH 3T3 fibroblast attachment, spreading, and cytoskeletal organization. *J Biomed Mater Res*. 1998;41:422-430. doi:10.1002/(SICI)1097-4636(19980905)41:3<422::AID-JBM12>3.0.CO;2-K
46. Philp AM, Raja S, Philp A, Ede MPN, Jones SW. The effect of vancomycin and gentamicin antibiotics on human osteoblast proliferation, metabolic function, and bone mineralization. *Spine (Phila Pa 1976)*. 2017;42(3):202-207. doi:10.1097/BRS.0000000000001712
47. Clarke B. Normal bone anatomy and physiology. *Clin J Am Soc Nephrol*. 2008;3:S131-S139. doi:10.2215/CJN.04151206
48. Buck DW, Dumanian GA. Bone biology and physiology: Part I. the fundamentals. *Plast Reconstr Surg*. 2012:1314-1320. doi:10.1097/PRS.0b013e31824eca94
49. Buckwalter JA, Glimcher MJ, Cooper RR, Recker R. Bone biology. Part I: Structure, blood supply, cells, matrix, and mineralization. *J Bone Jt Surg - Ser A*. 1995:1256-1275. doi:10.2106/00004623-199508000-00019
50. MARKSJR S, ODGREN P. Structure and Development of the Skeleton. In: *Principles of Bone Biology*. ; 2002:3-15. doi:10.1016/b978-012098652-1/50103-7
51. Jones AC, Arns CH, Sheppard AP, Hutmacher DW, Milthorpe BK, Knackstedt MA. Assessment of bone ingrowth into porous biomaterials using MICRO-CT. *Biomaterials*. 2007;28(15):2491-2504. doi:10.1016/j.biomaterials.2007.01.046